Structure–property relationships in perfectly alternating segmented polysulphone/poly(dimethylsiloxane) copolymers

D. Tyagi*, J. L. Hedrick‡, D. C. Webster§, J. E. McGrath and G. L. Wilkes**

Departments of Chemical Engineering, Chemistry and Polymer Materials and Interfaces Laboratory, Virginia Polytechnic Institute and State University, Blacksburg, VA 24061-6496, USA

(Received 12 May 1987; accepted 16 September 1987)

Well-defined perfectly alternating multiphase segmented polysulphone/poly(dimethylsiloxane) copolymers have been synthesized by the silylamine–hydroxyl coupling reaction and studied by thermal, mechanical and optical scattering methods. The results showed that by varying the length of the segments for each phase and their relative content, it is possible to alter the mechanical and thermal characteristics from those of a thermoplastic elastomer to a tough ductile transparent thermoplastic. The mechanical response was also shown to be influenced according to which phase was predominantly continuous. The evidence of microphase morphology was principally based on dynamic mechanical, small angle X-ray scattering (SAXS) and transmission electron microscopy (TEM) measurements. Differential scanning calorimetry (d.s.c.) scans showed the breadth of the high temperature transitions to span up to 60°C, reflecting the polydisperse nature of both oligomers. New results from SAXS analysis agree well with TEM measurements and indicate that the interfacial thickness parameter and degree of phase separation also show a composition and block length dependency for these copolymers. The interfacial thickness parameter, based on Koberstein's empirical method, was found to vary from 0.8 to 1.3 nm, depending on the composition.

(Keywords: block polymers; polysulphone; poly(dimethylsiloxane); phase separation)

INTRODUCTION

In recent years attempts have been made to obtain information regarding the morphological features of block and segmented copolymers. The techniques used for this purpose have included small-angle X-ray scattering (SAXS)[1-11], small-angle neutron scattering (SANS)[13-16], small-angle light scattering (SALS)[2,6,17,18], wide-angle X-ray scattering (WAXS)[1,2,5,6,10,17,19-21], nuclear magnetic resonance (n.m.r.)[22,23], infra-red spectroscopy (i.r. and *FT*i.r.)[2,24-29], optical microscopy[1,2,6,30], differential scanning calorimetry (d.s.c.)[1,5,12,23-25,31-33], scanning and transmission electron microscopy (TEM)[1,6,10,30,34-43] and dynamic mechanical analysis[75-78]. In general, the morphological results obtained from one approach can often be correlated with those obtained by another, unless the sample preparation methods for the two techniques are substantially different. This is especially true in the case of TEM and SANS. Attempts have been made to correlate the morphological evidence from these two techniques with the results obtained by SAXS analysis on bulk samples[44,45]. In many cases, if discrepancies occur they may well be due to different methods of sample preparation.

The technique of electron microscopy is very attractive since it provides a direct image for structural evidence. However, it is not without drawbacks. First, the particle size and its distribution should be larger than a few angströms in size. Second, electron microscopy is limited to the study of thin films or sections or replicas of free surfaces. If the film thickness is much larger than the dispersed domains, then an overlap of domain images results. Problems of this nature have often been overlooked. Similar problems can arise if a sample with lamellar morphology is not carefully prepared. Third, electron microscopy requires sufficient contrast in the electron micrographs in order to visualize the structures. Even for an ideal multiphase polymeric system with sharp phase boundaries, the electron and mass density differences are generally too low to be useful.

If sufficient amplitude contrast in a two-phase structure is not available, then the only alternative is to carry out selective staining (fixation) with heavy atoms such as osmium[46] or ruthenium[69]. Even if one can obtain sufficient contrast, the material must not also be rapidly degraded by the electron beam. In order to obtain a suitable thin polymeric film, in all the references mentioned above the technique of solution casting was

* Present address: Kodak Research Laboratory, 82-A236, Rochester, NY 14650, USA
‡ Present address: IBM Research Laboratory, K91/282, San Jose, CA 95193, USA
§ Present address: Sherwin-Williams Co., Technical Center, 10909 Cottage Grove Ave, Chicago, IL 60628, USA
** To whom correspondence should be addressed

0032-3861/88/050833-12$03.00

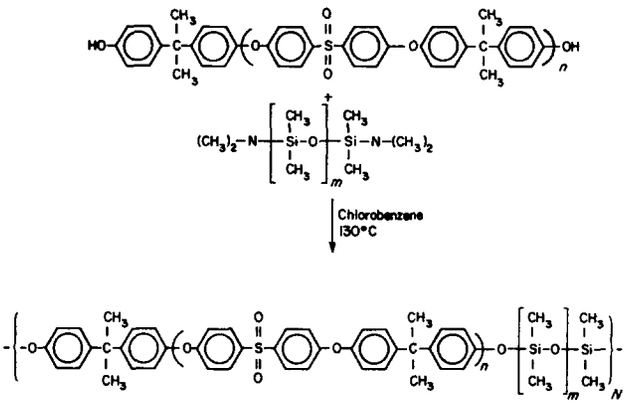

Scheme 1

generally employed. The other method is to ultramicrotome the as reacted or possibly moulded samples under cryogenic conditions[1,40]. It is quite conceivable that some of the above steps can lead to artefacts unrelated to the true morphology. For example, differences in the rates of solvent removal encountered in solution casting of thin films can be shown to have a marked effect on the morphological texture[71]. Alternatively, since the specific staining technique involves a chemical reaction, the nature and extent of the microphase separation can be influenced. Some success in morphological characterization has been obtained by the use of defocus electron microscopy, as proposed by Miles and Petermann[47]. However, Roche and Thomas[48] have reported that unless focusing parameters are sufficiently defined one may obtain ambiguous size determinations.

In the present work, structure–property relationships in perfectly alternating segmented copolymers based on soft poly(dimethylsiloxane) segments and hard glassy poly(arylene ether sulphone) segments[53] have been investigated (see *Scheme 1*). Since the mechanical and thermal properties of segmented materials are dictated by the morphological texture present in the sample, it was desirable to further characterize this morphology and to establish how it affects these properties. Polysulphone/poly(dimethyl siloxane) block or segmented copolymers were chosen for this investigation for several reasons. The most important is that there was an established route for the synthesis of well defined, perfectly alternating block copolymers[71]. The silylamine–hydroxyl condensation route employed for the synthesis in this study has been shown to be very facile for the formation of perfectly alternating block copolymers. Furthermore, each oligomer and hence each block can be characterized independently prior to copolymerization. The silicon–oxygen–carbon link between the block structure below has been demonstrated to be very stable to oxidation as well as surprisingly displaying very satisfactory hydrolytic stability[52,57,73].

The segmental arrangement is perfectly alternating in these copolymers since the hydroxyl terminated oligomer can react *only* with the silylamine terminated oligomers in the step-growth reaction. The distribution of both the soft and the hard segments in these materials is, therefore, subject only to the molecular weight distribution of the hydroxyl functional polysulphone and the PDMS oligomers. Note that this is not usually the case in the more widely studied segmented polymers.

The other important reason for the selection of polysulphone/polysiloxane (PSF/PSX) segmented copolymers in this study was because of the large differences in properties of the components involved, some example parameters being the glass transition temperature (-123°C for PSX vs. $+190$°C for PSF); solubility parameter, δ [$\delta_{PSX} = 7.3$ (cal cm^{-3})$^{1/2}$ and $\delta_{PSF} = 10.3$ (cal cm^{-3})$^{1/2}$] and the electron density, ρ ($\rho_{PSX} = 0.527$ me cm^{-3} and $\rho_{PSF} = 0.648$ me cm^{-3}). The electron and mass density difference already present between the two components allows the SAXS and TEM analysis to be carried out without any further modification.

The method of small-angle X-ray analysis was applied in this study, in addition to the TEM morphological investigations. An extensive investigation of many of the physical properties, including permeability, of similar copolymers has already been reported by Robeson *et al.*[50]. We have also included mechanical and thermal measurements on the copolymers in order to correlate the morphological results obtained from SAXS and TEM with the observed properties.

EXPERIMENTAL

Materials

Synthesis of bisphenol A polysulphone oligomers. Functionally terminated oligomers of bisphenol A-polysulphone were successfully synthesized by aromatic nucleophilic substitution using the *N*-methyl-2-pyrrolidone–potassium carbonate route[51]. Bisphenol A (Dow Chemicals) and 4,4′-dichlorodiphenylsulphone (Union Carbide) were reacted in the proper stoichiometric imbalance as determined by the use of the Carothers equation[72] to give the appropriate number-average molecular weight and, after acidification, two phenolic hydroxyl terminal groups[51,53].

Synthesis of dimethylamino-terminated poly(dimethylsiloxane) oligomers. The dimethylamino-terminated poly(dimethylsiloxane) oligomers were prepared by the anionic tetramethylammonium siloxanolates catalysed bulk equilibration of low molecular weight oligomers with the cyclic tetramer, D_4, as discussed elsewhere[52]. The precursor oligomer was obtained either from Union Carbide Corporation or Petrarch Systems Inc. It can be synthesized by capping silyl chloride end-blocked oligomers with dimethylamine in the presence of magnesium.

Synthesis of the polysulphone/poly(dimethylsiloxane) segmented copolymers. The perfectly alternating polysulphone/poly(dimethylsiloxane) segmented copolymers were synthesized in solution using Noshay's silylamine–hydroxyl condensation reaction[53-57] (see *Scheme 1*). The reaction was conducted in a 1 litre four-necked round-bottomed flask fitted with a mechanical stirrer, a Dean-Stark trap, condenser, thermometer, inert gas inlet, and an addition funnel. A typical reaction utilized to produce polysulphone/poly(dimethylsiloxane) block copolymer employed 22.3 g of 4900 $\langle M_n \rangle$ hydroxyl-terminated polysulphone oligomers placed in the flask with 500 ml chlorobenzene. The temperature was raised until the chlorobenzene began to reflux (132°C). Approximately 100 ml of solvent was removed

Table 1 Composition of various PSF/PSX copolymers synthesized

Sample	MW PSF/PSX	$[\eta]_{THF}^{25°C}$	PSX (wt%)
I	4900/4400	0.60	47
II	4900/12 800	0.60	72
III	9700/12 800	1.27	57
IV	9700/6700	0.78	41

from the Dean-Stark trap to dehydrate the system. This must be done to eliminate premature hydrolysis of the silylamine end groups. The 4400 dalton siloxane oligomer (20.0 g) was placed in an addition funnel and half the oligomer was added slowly to the solution and allowed to react until the evolution of amine (as detected by pH paper) had significantly decreased. At this point, the rest of the siloxane oligomer was slowly added in increments. A noticeable increase in the viscosity was observed as the stoichiometric point was approached, as expected. The reaction was allowed to continue at reflux temperatures for another hour. It was then cooled to room temperature, precipitated in a rapidly stirred 10-fold excess of methanol/isopropanol mixture, and dried for 24 h at 70°C in a vacuum oven.

It should be emphasized that the silicon–oxygen–carbon bond linking these segments is surprisingly stable hydrolytically, which is in contrast with the behaviour of this bond in small molecules[52-57,73]. Some important characteristics of the segmented copolymers synthesized are listed in *Table 1*.

The mechanically recovered yields were all at least 90% and all of the copolymers formed clear solutions in chloroform and other appropriate solvents. This was important since the presence of homopolymers produces hazy solutions, even at quite low levels. Analysis of the copolymers by ^1H n.m.r. indicated that quantitative siloxane incorporation had been achieved.

Film preparation

Well formed compression moulded films for the PSF5000/PSX5000, or higher M_n segmented copolymers are essentially impossible to obtain because the microphases remain separated, even in the melt, up to very high temperatures[79]. Since the melt viscosity of these systems were very high, the films in this study were obtained by a solution casting method from a 10% (w/v) filtered chloroform solution. These thin films were carefully dried under vacuum at 80°C for 24 h in Teflon moulds.

Analysis of oligomers and polymers

Titration of functional oligomers. The number-average molecular weight of these difunctional oligomers was determined by titration of the reactive end groups. The titrations of functional oligomers were carried out using a computer-interfaced Fisher Scientific Titrimeter II automatic titrator operating in the automatic endpoint seeking (AEP) mode. A standard calomel electrode was used with a double junction reference. The electrodes were stored in a pH 4.0 buffer. The electrometer was calibrated according to the manufacturer's instructions. A 10 ml burette was used for all titrations. The hydroxyl-terminated poly(aryl ether sulphone) oligomers were titrated with 0.2 M aqueous tetraethylammonium hydroxide in 20 ml of either dry *N,N*-dimethylformamide (DMF) or *N,N*-dimethylacetamide (DMAC) as reported previously[58]. The dimethylamino-terminated poly(dimethylsiloxane) oligomers were titrated with 0.1 M alcoholic HCl in 100 ml of dry isopropanol.

Intrinsic viscosity determinations. Intrinsic viscosities of the polymers were determined using a Cannon-Ubbelohde dilution viscometer. Four concentrations of the polymer solution in the appropriate solvent were used for the measurements. All determinations were made at 25°C.

G.p.c. chromatograms were obtained using a Waters Model 150C instrument, operated at room temperature with Styrogel columns of 10^5, 10^4, 10^3 and 500 A in THF with a flow rate of 1 ml min^{-1}. Thermal analysis of the copolymers were studied with a Perkin-Elmer System 2 DSC and TMA at a heating rate of 10°C min^{-1}. The load used during the TMA penetration–temperature studies was 10 g.

Mechanical measurements. Dog-bone specimens were cut from the films for the mechanical testing of these copolymers. Mechanical measurements included stress–strain, stress relaxation, tensile hysteresis and permanent set behaviour. These tests were performed on an Instron Model 1122. All stress–strain and hysteresis measurements were carried out at a strain rate of 200% per minute, based on the initial sample length.

Dynamic mechanical spectra were determined either on a Rheovibron Model DDV II-C at 110 Hz or a Polymer Laboratories DMTA at 1 Hz. The rate of heating during these experiments was 2°C min^{-1}.

X-ray analyses. Small-angle X-ray experiments were carried out using a standard Kratky camera. For the Kratky camera experiment, the X-ray source was a Siemens Ag Cu 40/2 tube, operated at 40 kV and 20 mA by a GE XRD-6 generator. Copper Kα radiation of wavelength 0.1542 nm was used in conjunction with a nickel filter. The sample to detector distance was 214 mm and a step motor-proportional controlled counter was used to scan the small-angle range. The X-ray data were analysed by a modified Vonk's program[80].

Transmission electron microscopy. Transmission electron microscopy (TEM) was performed on ultra-thin cast films of the siloxane containing block copolymers to directly observe the nature of the microphase separation in these block copolymers. Staining of either phase was unnecessary due to the large difference in electron density between the poly(dimethylsiloxane) and the polysulphone. The films were prepared by casting a 5% chloroform solution of the polymer on water. The film was then directly transferred to a 150 mesh copper grid. The bright-field images or micrographs were obtained using both a Jeol 100C TEM and a Philips EM-420 STEM, both operating at 80 keV. The Philips instrument has a resolution of 0.15 nm in the TEM mode. In order to obtain better contrast in the bright-field images, an objective aperture of 50 μm was used for all images with magnification over 100 000. However, it must be realized that the morphology observed in thin solution-cast films may well be different from the true bulk morphology

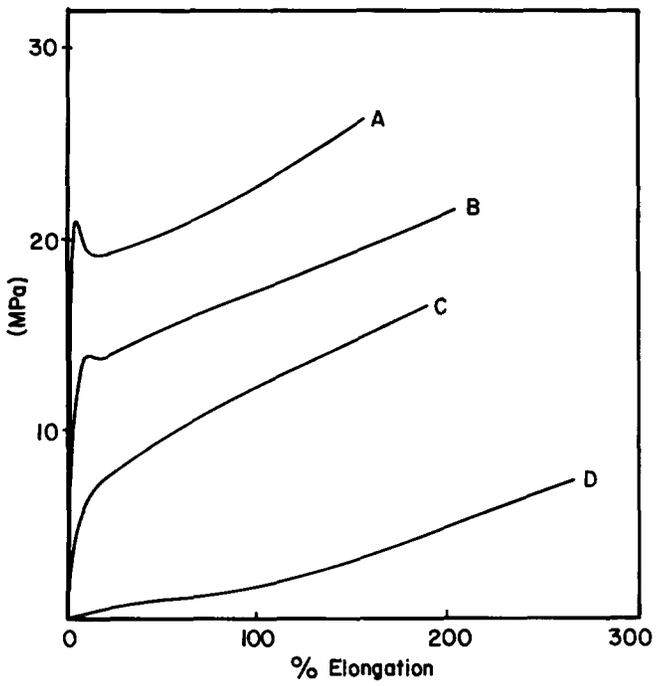

Figure 1 Stress–strain curves for: A, PSF9700/PSX6700; B, PSF4900/PSX4400; C, PSF9700/PSX12800; D, PSF4900/PSX12800

which may exist in the thicker cast films used for mechanical testing.

RESULTS AND DISCUSSION

Mechanical and thermal analysis

The nature of solvents utilized in solution casting of block copolymers is known to have a strong influence on their solid state structure and physical behaviour[73]. For example, the work of Robeson *et al.*[50] has clearly demonstrated that the mechanical response of the subject copolymers is significantly affected by the choice of the solvent employed in the solution casting process. When more thermodynamically favourable solvents for polysulphone were used, the resulting mechanical properties were more characteristic of polysulphone (higher modulus etc.). Robeson's results indicate that the choice of solvents influences the amount and nature of the phase separation, which in turn alters the morphological texture in the segmented copolymers. This conclusion was further verified by determining the mechanical strength of films swollen in a solvent for polysiloxane but a non-solvent for polysulphone. Depending upon the amount of swelling, different mechanical strengths were obtained, indicating again that morphology can be affected by the choice of the solvent. Similar conclusions about the effect of solvent on morphology have been reached by others, also for different block copolymers[12,73]. Although such effects are very important, the casting solvent was limited to the relatively 'good' solvent chloroform.

The engineering stress–strain curves for various copolymer films prepared from solution casting with chloroform are shown in *Figure 1*. All the curves were examined up to the fracture strength of the specimen. The initial modulus and other mechanical characteristics are presented in *Table 2*. As observed previously, the mechanical behaviour is dictated by the volume fraction of polysiloxane present in the copolymer. At high siloxane content (70 wt%), a more pronounced elastomeric character is evident for the copolymer, no doubt due to the more continuous nature of the soft segments.

A comparison of the curves in *Figure 1* shows that by increasing the polysiloxane segment length at constant PSF molecular weight, the initial modulus and tensile strength are decreased. The ultimate elongation increases slightly over the composition range reported when the siloxane block length and content are increased. On increasing the PSF segment length (and content) for the same PSX segment length (curves B and C) an exact opposite trend is observed. Below 50 wt% polysiloxane, a yield point is observed between 5 and 10% elongation, which suggests some continuity of the polysulphone phase. The yield strength and the elongation at the yield point can be correlated with the extent of polysulphone continuity in the segmented copolymer. For example, the magnitude of the yield stress is higher and the yield point is observed at lower elongations as the sulphone content (and hence its continuity in the copolymer) is increased. The ultimate tensile strength over the composition range increases from about 7 to 30 MPa as the PSF is increased from 28 to 59 wt%.

The dynamic mechanical storage modulus and tan δ obtained for these systems are shown in *Figure 2*. The results strongly indicate a two-phase nature for the materials, which undoubtedly arises due to the large solubility parameter difference between the two block components. All samples show a transition near $-115°C$, which corresponds to the glass transition of the

Table 2 Summary of mechanical properties for solvent-cast PSF/PSX copolymers

Sample	MW PSF/PSX	Tensile strength (MPa)	% Elongation at break	Modulus (MPa)	Yield point
I	4900/4400	20.9	200	35.3	Yes
II	4900/12800	6.6	260	0.2	No
III	9700/12800	14.3	180	17.4	No
IV	9700/6700	29.5	200	90.6	Yes

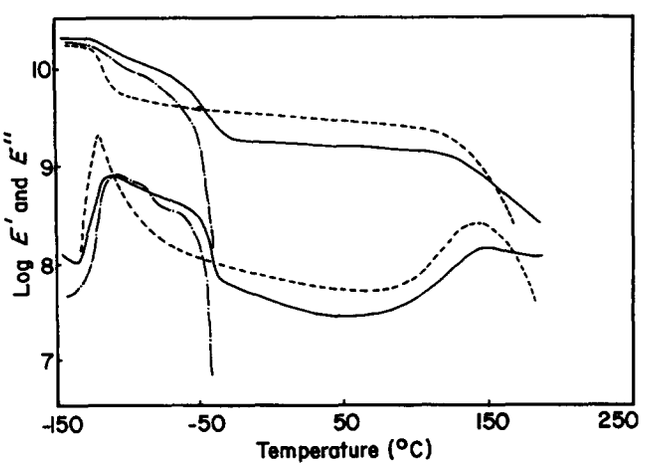

Figure 2 Dynamical mechanical measurements for: ——, PSF4900/PSX4400; ——, PSF9700/PSX12800; –·–·–, PSF4900/PSX12800

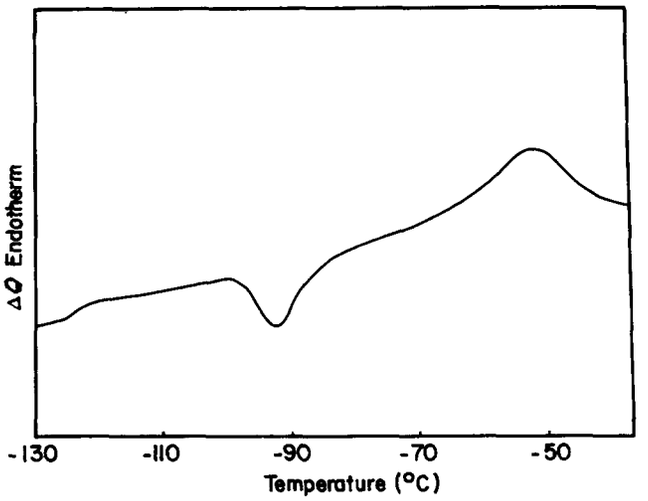

Figure 3 Low temperature d.s.c. scan for PSF9700/PSX6700 copolymer

poly(dimethyl siloxane). The position of T_g for PSX does not appear to be dependent on the molecular weight of either component. This agrees with a study by Yilgor *et al.*[81], which indicated that the T_g of PSX functional oligomers reaches a plateau value of -123°C at number-average molecular weights of about 2000. Samples PSF4900/PSX12800 and PSF9700/PSX12800, which have a high siloxane content, show the presence of a crystalline transition in addition to the glass transition. This siloxane crystallinity is not evident at low siloxane content compositions or in copolymers for which the molecular weight of the siloxane segments is relatively small (<5000). This inability to crystallize results from the restrictions imposed on the chains by the chemical bonding between the segments[82]. The $\tan\delta$ peak corresponding to the T_g of the siloxane is also found to be suppressed when the crystalline transition is present for that phase. In such cases, the intensity of the peak should be proportional to the amount of amorphous siloxane chains present in the system.

The dynamic mechanical results also indicate that the storage modulus in the rubbery plateau is dependent on the polysulphone content incorporated in the copolymer. The rubbery plateau modulus is the highest for the copolymer in which the level of polysulphone was highest and can be correlated with the content and the continuity of the polysulphone phase. As is evident from *Figure 2*, no sub T_g transition for PSF is observed near -100°C. It has been determined by others[60] that this transition is very dependent on molecular weight and is not observed if the molecular weight of the PSF is low.

For sample PSF4900/PSX12800 the decrease in the storage modulus is very sharp after the melting transition for the siloxane. This suggests that for this copolymer the PSF is the dispersed phase and only serves to provide physical junction points for the pseudo network structure. This is consistent with the relatively high volume fraction of siloxane in this copolymer. In the other copolymers, the composition is such that additional continuity in the polysulphone phase is present. As a consequence, the storage modulus does not fall off as rapidly above the T_m of siloxane.

The glass transition associated with the hard phase is found to be dependent on the composition of the copolymer at the block length examined. This transition is found to increase with the polysulphone block length in the copolymer. For materials with high PSF content, not only is the height of the tan δ peak greater, but the peak is located at a somewhat higher temperature. The transition for the hard segments lies in the range 140 to 155°C, depending on the molecular weight of the blocks. Robeson *et al.*[59] demonstrated in their work that for copolymers with about 50 wt% polysulphone, the T_g for the hard phase was dependent on the block molecular weight. It is apparent that an uppermost T_g of 190°C was approached only when the polysulphone number-average molecular weight was in excess of 12 000. Indeed, we have synthesized a copolymer based on a 17 000 molecular weight PSF, and a 4400 molecular weight of PSX and this indicated a well defined PSF glass transition at 189°C[83]. This result along with those of Robeson *et al.* imply that there is either a large degree of mixing or a large interfacial region between the two segments in these materials. The extent of mixing or the interfacial region is a function of the respective chain lengths of the precursor materials incorporated in the copolymer. This is apparent since the glass transition behaviour corresponding to the hard phase is composition-dependent.

The thermal response of these materials from the second d.s.c. scan shows a behaviour similar to that observed in the dynamic mechanical experiments. The low-temperature glass transition associated with the siloxane chains is observed near -123°C. A crystallization and melting transition was also indicated near -100°C and -60°C, respectively. As an example, a thermal scan for sample PSF9700/PSX6700 is presented in *Figure 3*. The results for the various transitions observed from the d.s.c. scans of these copolymers are reported in *Table 3*. Comparing the results with those from dynamic mechanical experiments, it is evident that the transition temperatures are shifted somewhat on the temperature scale because of frequency dependence. However, the same general conclusions regarding morphological character can be reached by both analyses. The glass transition temperature for the polysulphone interestingly shows a strong unexpected dependence on composition whereas the general behaviour of the soft segment is more as expected. The most outstanding feature in the thermal scans is the breadth of the hard segment (PSF) transition observed, as is indicated in *Figure 4*. The breadth is observed to span nearly 60°C! The T_g values indicated in *Table 4* correspond to the midpoint of the transition. This broad glass transition for polysulphone suggests that there is some large-scale mixing or interfacial region development between the hard and soft segments. It may also reflect the relatively polydisperse nature of both starting oligomers.

These results are somewhat surprising in light of the high solubility parameter difference existing between the

Table 3 Influence of composition and segment molecular weight on various poly(dimethylsiloxane) transitions observed by d.s.c.

Copolymer	MW PSF/PSX	T_g (°C)	T_c (°C)	T_m (°C)
I	4900/4400	−125	-	-
II	4900/12800	−126	−99	−62
III	9700/12800	−124	−86	−57
IV	9700/6700	−128	−100	−60

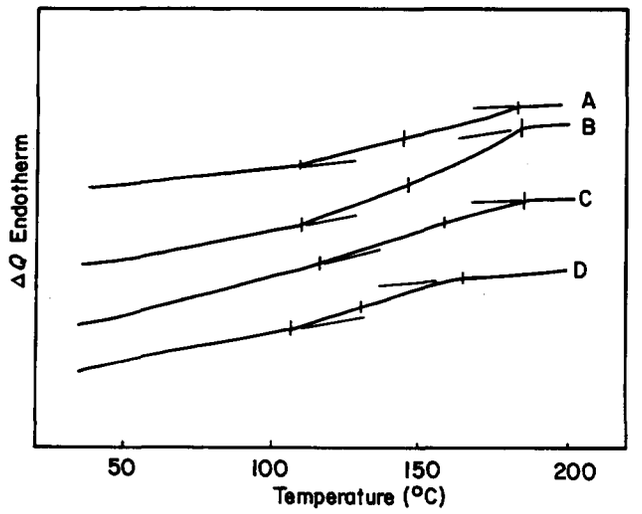

Figure 4 High temperature d.s.c. scans showing the glass transition for the hard segments. A, PSF9700/PSX6700; B, PSF9700/PSX12800; C, PSF4900/PSX12800; D, PSF4900/PSX4400

Table 4 Influence of copolymer composition and segment molecular weight of polysulphone transition location and breadth observed by d.s.c.

Sample	MW PSF/PSX	T_g (PSF) °C From	To	Midpoint
I	4900/4400	107	166	131
II	4900/12800	118	185	160
III	9700/12800	110	184	146
IV	9700/6700	110	182	142

two segments. One explanation for this behaviour could be the large distribution of hard and soft segment lengths which may be present in the system related to the polydispersity question raised above. In order better to understand this, there was a need to obtain information regarding the extent of phase mixing. This was achieved with the aid of small-angle X-ray scattering (SAXS).

SAXS analysis

As mentioned previously, small-angle X-ray scattering can be employed as a very valuable tool for the characterization of two-phase microstructures in segmented thermoplastic elastomeric materials. By utilizing this technique, the analysis can provide measurements on the interdomain spacing, interfacial boundary thickness and the degree of microphase separation. The determination of these morphological parameters by SAXS is relatively straightforward, as explained elsewhere[11,61-66,70].

Interdomain spacing

The simplest approximation to determine the interdomain spacing is by the application of Bragg's Law. As the angular position of the maximum in the scattering profile is directly related to the interdomain spacing, d, Bragg's Law for first-order diffraction can be written as:

$$s = \frac{2\sin\theta}{\lambda} = \frac{1}{d} \quad (1)$$

where θ is the internal scattering or 'Bragg' angle, λ is the wavelength and s is the magnitude of the reciprocal lattice vector.

The slit-smeared X-ray scattering profiles for these polysulphone/polysiloxane segmented copolymers are presented in *Figure 5*. All the curves are characterized by the presence of a maximum followed by a sharp decrease in the scattered intensity. The position of the maximum in the intensity profile is dependent on the composition of the copolymer in terms of the molecular weight of the soft and hard segments employed.

The same trend is observed for the collimation corrected intensity profiles. *Figure 6* presents the

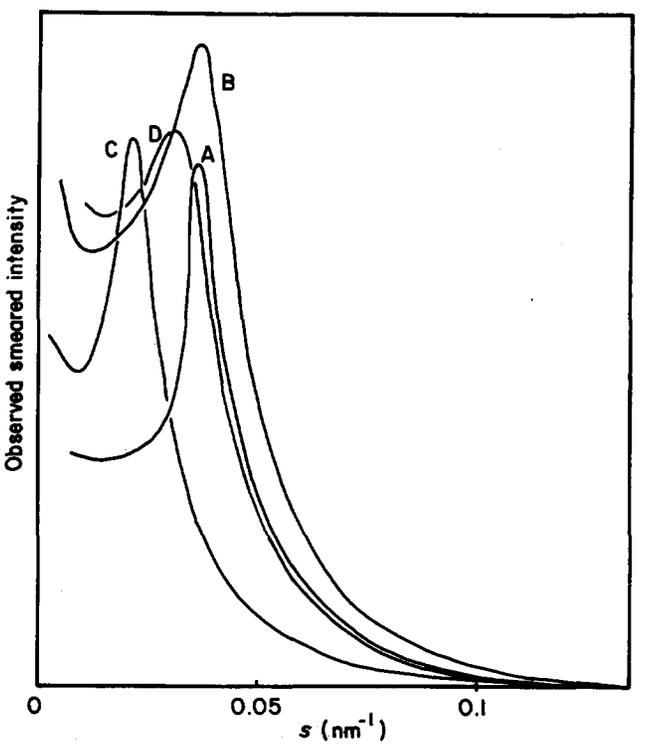

Figure 5 Smeared small-angle X-ray scattered intensity profiles for: A, PSF4900/PSX4400; B, PSF4900/PSX12800; C, PSX9700/PSX12800; D, PSF9700/PSX6700

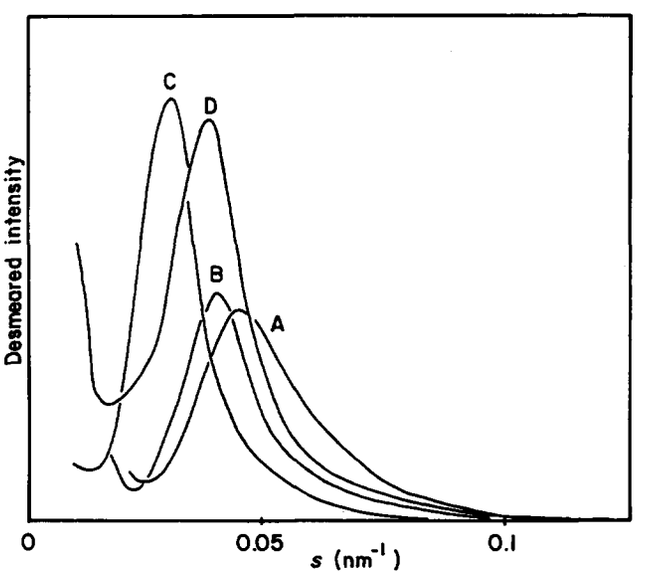

Figure 6 Desmeared small-angle X-ray scattered intensity profiles for A, PSF4900/PSX4400; B, PSF4900/PSX12800; C, PSF9700/PSX12800; D, PSF9700/PSX6700

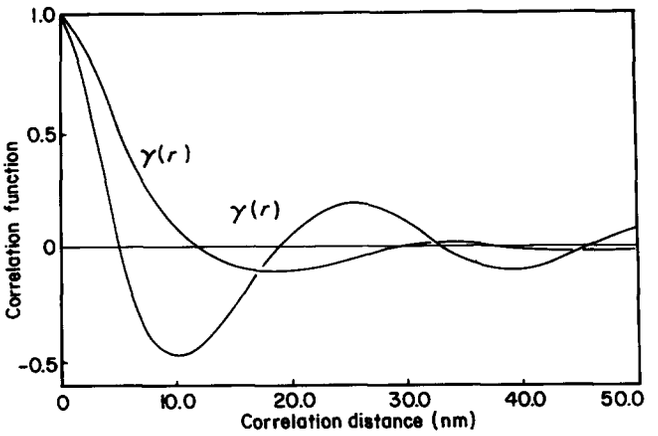

Figure 7 One- and three-dimensional correlation functions for PSF9700/PSX6700

Table 5 SAXS interdomain spacing in PSF/PSX copolymers (nm)

Sample	Bragg's law	$\gamma(x)^a$	$\gamma(r)^b$
4900/4400	18.0	17.0	25.0
4900/12800	23.5	21.0	27.5
9700/12800	34.8	31.0	40.0
9700/6700	26.5	24.0	31.0

[a] $\gamma(x)$ is the 1-D correlation function calculated from scattering profile
[b] $\gamma(r)$ is the 3-D correlation function calculated from scattering profile

desmeared data for the segmented copolymers under investigation. This step is necessary because the determination of the interdomain spacing through the application of Bragg's Law requires the use of collimation-corrected intensities. A comparison of smeared and desmeared intensity profiles reveals that the collimation correction procedure moves the position of the maximum to a higher scattering vector, as is the usual case.

Through the use of the corrected intensity profiles and Bragg's Law, the interdomain spacings, d, were determined. The Bragg or the interdomain spacing calculated ranges from 18.5 nm for copolymer PSF4900/PSX4400 to nearly 35.0 nm for the copolymer PSF9700/PSX12800.

The interdomain spacings were also calculated following the determination of correlation functions. As mentioned elsewhere[11], the correlation function $\gamma(r)$ contains all the information about the particle (domains) shape and their spatial distribution that can be obtained from the scattering profile. This function can also be viewed as the probability function for a rod of length r to have both its ends embedded in a phase of the same electron density. Therefore, a peak or maximum in the correlation function corresponds to a high probability and hence provides information on the periodicity or correlation distance in the local density fluctuations that arise from the microphase morphology. This correlation distance [the first maximum in $\gamma(r)$] can be viewed as a good estimate of the interdomain spacing.

The correlation functions for sample PSF9700/PSX6700 are presented in *Figure 7*. The three-dimensional correlation functions for these copolymers show only a weak maximum. The one-dimensional correlation function, on the other hand, shows a series of well defined maxima which damp off gradually with increasing distance. The results of the interdomain spacing determined from the one- and three-dimensional correlation functions along with those obtained from Bragg's Law are listed in *Table 5*. The d spacing obtained through the various methods, although not the same, clearly follow a similar pattern. Nevertheless, for all cases, the position of the first maxima in the one-dimensional correlation function gives a value which is close to but lower than the value obtained from Bragg's Law.

The results obtained here can be explained with the aid of *Figure 8*, which represents the one-dimensional schematic of a two-phase morphology. It is clear from the schematic that the interdomain spacing from the 1-D correlation function would be dependent on the conformations of the hard and soft segments. If, for a constant hard block length, the molecular weight of the soft segments is reduced, then the corresponding value of the interdomain spacing would also be lowered. For sample PSF4900/PSX4400 an interdomain spacing of 16.5 nm is observed. This distance increases to 22.0 nm when the molecular weight of the PSX alone is increased in sample PSF4900/PSX12800. Similarly, if the length of the hard segment is increased, while keeping the molecular weight of the soft siloxane segment the same, a comparison of samples PSF4900/PSX12800 and PSF9700/PSX12800 also shows a further increase to 31.0 nm. To a first approximation, if the square root of the mean square end-to-end distance for the siloxane chains is calculated and subtracted from these interdomain spacings, then an average size estimate of the polysulphone phase can be estimated. These calculations have been carried out and indicate that the size of the PSF phases nearly doubled as its molecular weight was increased by about 100%, a higher value than would be expected based on Gaussian chain consideration.

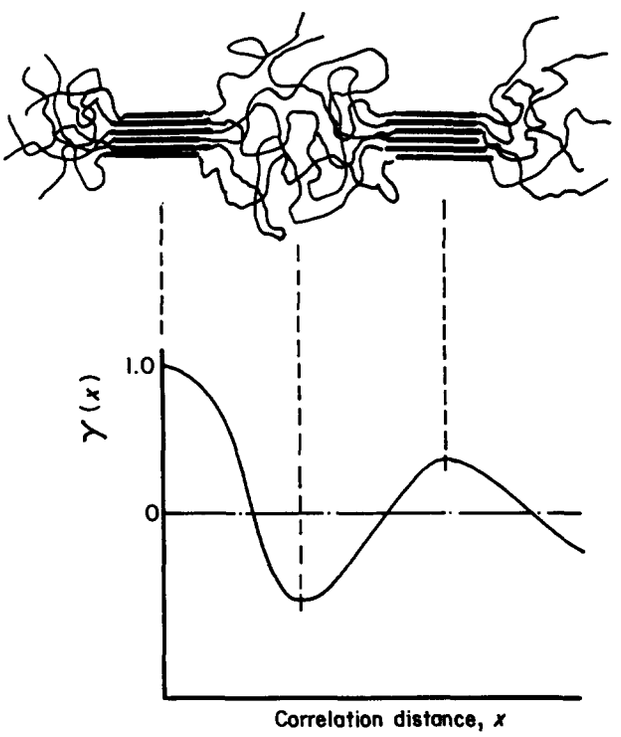

Figure 8 Simplified schematic showing the interdependence of interdomain spacing and correlation distance to the first maxima. For simplicity, the hard segments have been represented as 'sticks'

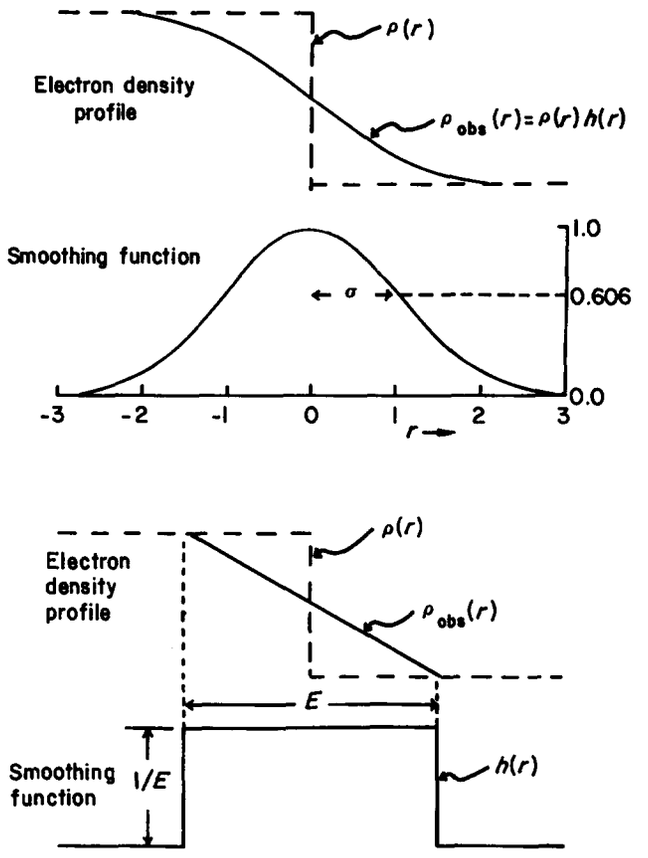

Figure 9 Representation of smoothing function for sigmoidal and linear gradient across the interface [Reproduced from Koberstein, J. T., Morra, B. and Stein, R. S. *J. Appl. Crystallogr.* 1980, **13**, 34 by permission of Munksgaard©]

However, these results are probably caused by corresponding changes in the morphological texture, i.e. spherical domain morphology, cylindrical domains or lamellar, which is dictated by the composition ratio. Since there is a large distribution of PSF segment lengths, it may be possible for the resulting copolymers to display considerable interfacial boundary thickness. The calculation of the interfacial thickness parameter, σ, based on the deviation from Porod's law is therefore now discussed.

Porod's behaviour and diffuse phase boundary structure

For an ideal case of a two-phase system with sharp phase boundaries, the scattering at high angles can be described by Porod's law:

$$\lim_{s\to\infty} I_{\text{ideal}}(s) = \lim_{s\to\infty} I_p(s) = \frac{k_p}{s^4} \qquad (2)$$

where K_p is the Porod constant and is related to the specific surface of the dispersed particles. In other words, a plot of $I(s)\cdot s^4$ vs. s^2 (also referred to as a Porod plot) would have zero slope at high angles. The factors causing deviation from Porod's behaviour generally fall into two categories: those which give rise to a positive slope (or positive deviations) in a Porod plot at high angles include thermal density fluctuations, onset of wide-angle scattering and dissolved segments of one type in the other phase; more importantly, negative deviations from Porod's behaviour occur when diffuse phase boundaries are present.

In order to account for those factors which cause these deviations, Ruland modified Porod's law to obtain:

$$\lim_{s\to\infty} I_{\text{obs}}(s) = I_p(s)\cdot H^2(s) + I_B(s) \qquad (3)$$

The additional term $I_B(s)$ is the result of contributions to the intensity due to local thermal fluctuations in the system. Various methods have been proposed to calculate $I_B(s)$ and have been discussed elsewhere[11,64]. In summary, these methods require curve fitting at high angles, where the term $H^2(s)$ goes to zero. The term $H^2(s)$ is the Fourier transform of a function which accounts for the deviations from sharp phase boundaries in an ideal system. Therefore, this function depends upon the form of the electron density profile across the interface. By assuming, say, a sigmoidal gradient, one can make at least a qualitative comparison of the interfacial thickness in two-phase materials. The two most commonly assumed profiles for electron density across the interface along with the smoothing functions are given in *Figure 9*. For a sigmoidal gradient, the smoothing function is Gaussian in nature and the standard deviation, σ, provides a measure or index of the interfacial thickness. As compared to the linear gradient assumption, the sigmoidal gradient one has considerable justification based on Helfand's theoretical prediction[68].

For the slit smeared scattering profiles, equation (3) is not valid. The corresponding equation is given as:

$$\lim_{s\to\infty} \tilde{I}_{\text{obs}}(s) = \exp(p^2s^2)\tilde{I}_p(s)\cdot F(\sigma, s) + \tilde{I}_B(s) \qquad (4)$$

where p, the standard deviation for the Gaussian function goes to zero in the limiting case of infinite slits. The factor F is the analogue of $H^2(s)$ for the slit-smeared data. It should also be mentioned that according to Porod's law, when using smeared intensities, the plot does not diminish as the fourth power of the scattering vector s but rather as the third power[61]. The background intensity, $I_B(s)$ for the smeared profile is calculated in a similar fashion to the pinhole intensity profiles and has been discussed in detail by Koberstein[65,67].

The function F is dependent on the form of the electron density profile existing across the interface boundary. In general, the intensity expressions do not permit a direct estimation of σ by analytical methods. However, by making approximations for the function F, the corrected scattering profile can be reduced to such a form that graphical determination of σ is possible. Some forms of F are listed in *Table 6* and details of the graphical procedures required to calculate σ are summarized in *Table 7*. Koberstein *et al.*[65,67] have recently reported on the validity of these approximations and have also proposed a self-consistency test.

The Porod behaviour of these PSF/PSX segmented copolymers is given in *Figure 10*. All plots show the negative deviations from Porod's law, implying the

Table 6 Forms of $F(s)$ for slit collimation assuming a sigmoidal gradient across the interface

Bonart	$\exp(-4\pi^2\sigma^2s^2)$
Ruland	$(1-8\pi^2\sigma^2s^2)$
Koberstein	$\exp[-38(\sigma s)^{1.81}]$
Exponential	$\exp(-8\pi^2\sigma^2s^2)$
Helfand	$(\sqrt{12\pi}\sigma s)^2\,\text{cosech}^2(\sqrt{12\pi}\sigma s)$
Roe	$3.3x^{1.8}\exp(-1.9x)s^3$ where $x=\sqrt{12\pi}\sigma s$

Table 7 Estimation of interfacial thickness parameter for sigmoidal gradient (slit collimation)

Approximation	Plot required	Estimation of parameter
Ruland	$s \cdot \tilde{I}_{corr}$ vs. $1/s^2$	$\sigma^2 = -$intercept/slope $4\pi^2$
Koberstein	$\ln(s^3 \cdot \tilde{I}_{corr})$ vs. $s^{1.81}$	$\sigma^{1.81} =$ slope/38
Exponential	$\ln(s^3 \cdot \tilde{I}_{corr})$ vs. s^2	$\sigma^2 = -$slope/$8\pi^2$
Bonart	$\ln(s^3 \cdot \tilde{I}_{corr})$ vs. s^2	$\sigma^2 = -$slope/$4\pi^2$
Roe	$\ln(\tilde{I}_{corr} \cdot s^{1.8})$ vs. s	$\sigma = -$slope/$1.9\sqrt{12\pi}$

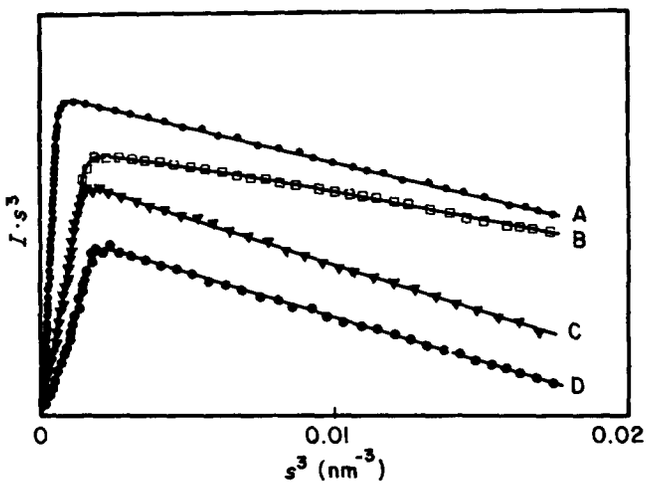

Figure 10 Porod's law behaviour for the smeared X-ray intensities indicating the presence of diffuse interfacial region. A, PSF4900/PSX4400; B, PSF4900/PSX12800; C, PSF9700/PSX12800; D, PSF9700/PSX6700

presence of an interfacial boundary region in all samples. The thickness of the interfacial boundary was calculated by several different techniques, assuming a sigmoidal electron density profile.

The diffuse boundary thickness parameter, σ, was estimated by utilizing the graphical methods of Ruland, Bonart and Koberstein. The results obtained for the sigmoidal boundary thickness parameter are presented in *Table 8*. For all samples the diffuse boundary width obtained by Bonart's method was the largest, followed by the approximations of Koberstein, the exponential treatment and, finally, Ruland's method, which gave the smallest value of σ. These differences are a consequence of the different ranges of validity for each method. In order to ensure that the range of s utilized in the determination of slope etc. was correct, the self-consistency test was carried out and the results are presented in *Figure 11*. This plot has been used by Koberstein *et al.*[67] in order to determine the range of validity of the different forms of F listed in *Table 6*. The ratio $\sigma_{meas}/\sigma_{true}$ was determined and plotted against a dimensionless quantity σs. However, in most cases σ_{true} is not known. A close look at the plot reveals that Koberstein's empirical method is closest to σ_{true}. Therefore, in *Figure 11*, the value of σ obtained by Koberstein's method was used instead. The resulting ratios were then calculated and recorded on the plot. These ratios were found to be close to the predicted behaviour, indicating that the choice of region selected for the determination of slope in the corresponding plots was correct. The value of σ obtained for these copolymers indicates that the interfacial thickness present in these systems is larger than that obtained for segmented polyurethanes by other workers and is closer to those obtained for block copolymers (the value of σ has been reported to be nearly 1.0 nm for PTMO/MDI/BD based polyurethanes and 1.2 to 1.3 nm for SBS type triblock copolymers[2,4,7]).

Degree of phase separation

The extent of phase separation in a system can be determined from a calculation of the mean square density fluctuation, or variance. For an ideal case where there is complete phase separation and a diffuse boundary is not present, the electron density variance is given by:

$$\overline{\Delta\rho_c^2} = \sum_i^N \phi_i(\rho_i - \bar{\rho})^2 \quad (5)$$

where ϕ_i is the volume fraction, ρ_i is the electron density for the ith phase and ρ is the mean electron density. The calculation of ρ can be carried out for each phase by knowing the chemical composition and the mass density for that phase. However, for real systems the electron density variance is lower owing to the presence of diffuse phase boundaries and mixing within phases. The electron density profile given in *Figure 12a* corresponds to one such real system when the thermal density fluctuations within the phases, diffuse phase boundaries and the mass density differences due to the domains are considered. If the thermal density fluctuations are removed, as

Table 8 Determination of σ (nm) by various approximations

Sample	Ruland	Koberstein	Bonart	Exponential
4900/4400	0.7	1.3	1.4	1.0
4900/12800	0.5	0.8	0.9	0.6
9700/12800	0.6	1.0	1.2	0.8
9700/6700	0.7	1.2	1.3	0.9

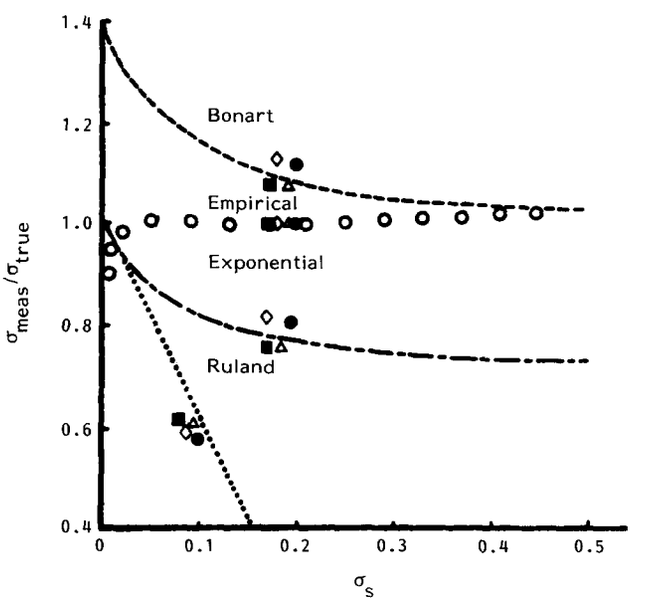

Figure 11 Consistency check used to test the validity of the choice of region selected for interfacial thickness determination. ●, PSF4900/PSX4400; ■, PSF4900/PSX12800; ◇, PSF9700/PSX12800; △, PSF9700/PSX6700

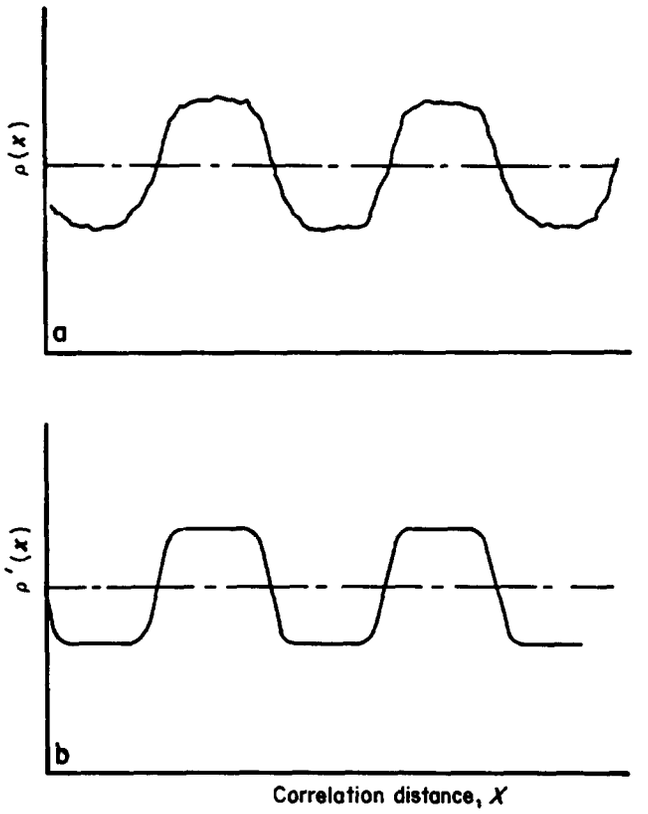

Figure 12 Schematic for the electron density profiles in: (a) real system; (b) same, after thermal density fluctuations are removed

described earlier, the electron density profile that results can be approximated by *Figure 12b*. This variance calculated for a real system holds the information on the degree of phase separation for that material.

The experimental determination of electron density variance can be carried out by using the relations already developed. From the profile which has been corrected for the thermal density fluctuations, the electron density variance, $\overline{\Delta\rho^{2'}}$, is determined by:

$$\overline{\Delta\rho^{2'}} = K\int_0^\infty I_{obs}\cdot s^2 ds \qquad (6)$$

where K is a constant which includes the Thomson scattering factor for an electron.

A comparison of $\overline{\Delta\rho^{2'}}$ and $\overline{\Delta\rho_c^2}$ can provide some information regarding the degree of phase separation. The ratio

$$0 < \overline{\Delta\rho^2}/\overline{\Delta\rho_c^2} < 1 \qquad (7)$$

provides a measure of the degree of overall phase separation. If the components are completely separated, then the ratio assumes a value of unity. The value of this ratio decreases if any interfacial mixing exists in the system.

The experimental electron density variance was calculated from the scattering profile presented in *Figures 5* and *6*. The theoretical electron density variance were determined from the knowledge of the chemical composition and mass density for the phases involved. The results are presented in *Table 9* and demonstrate that the experimental variance is much smaller than the theoretical variance for all the copolymers. This suggests that a significant amount of segmental mixing occurs in these copolymers. However, these values should be treated with caution because of the possible errors which are inherent in their determination. These errors have been discussed elsewhere in detail[11]. At this point it is sufficient to say that these errors arise since mass density of the segments is generally not available in the *copolymer* state, coupled with the fact that hard segment 'impurities' exist in the soft matrix, and vice versa, contribute to the intensity profile which gives rise to positive deviations from Porod behaviour[11,64]. Also, the results give a ratio of experimental to theoretical variance which is less than unity. The ratio was smallest for PSF4900/PSX4400, which indicates the highest degree of mixing. Sample PSF4900/PSX12800, on the other hand, had the largest ratio, indicating the least amount of segmental mixing. The results also show that the degree of phase separation can be improved by increasing the molecular weight of the soft segment. However, these conclusions should be viewed cautiously since the amount of interfacial region per unit volume is also reduced as the molecular weight of one component is increased.

Let us now summarize the morphological information obtained thus far. The thermal and dynamic mechanical studies support the X-ray findings that there is a surprisingly large-scale mixing of the hard/soft segments present in these copolymers. This mixing could be present either within each domain or at the interfacial region separating the two phases. The SAXS results appear to favour the latter rationalization. These results are rather surprising in the light of the large solubility parameter difference which exists between the two segment types. Even in the melt, these PSF/PSX segmented copolymers maintain their two-phase structure. However, it is possible that a large interfacial region could exist in these materials if the distribution of the hard segment lengths is large. The polydispersity of the PSF oligomers was found to be 2.2 by g.p.c., based on polystyrene standards. Assuming a polydispersity of 2.0, the breadth of the molecular weight distribution can be estimated from the relation:

$$\frac{\sigma}{\langle i\rangle} = \left(\frac{\langle i\rangle_w}{\langle i\rangle_n} - 1\right)^{1/2} \qquad (8)$$

The value of this ratio, determined from the above expression, is found to be 1. This implies that for a 5000 $\langle M_n\rangle$ PSF oligomer, 95% of the hard segments have their molecular weight between 0 and 10000; and 99.9% have their molecular weight between 0 and 20000! This suggests that there is indeed a large distribution of hard segment lengths present in these materials which may help to explain the observed large interfacial region. However, the two segments involved still maintain a two-phase structure in the melt, owing to the large solubility parameter difference between them and the small, but

Table 9 Degree of phase separation by electron variance method

Sample	MW PSF/PSX	$\overline{\Delta\rho_c^2}^a \times 10^3$	$\overline{\Delta\rho^{2'}}^a \times 10^3$	$\overline{\Delta\rho^{2'}}/\overline{\Delta\rho_c^2}$
I	4900/4400	3.682	0.90	0.25
II	4900/12800	2.628	1.20	0.46
III	9700/12800	3.460	1.30	0.38
IV	9700/6700	3.684	1.20	0.35

[a] Electron density in (m-electron cm^{-3})

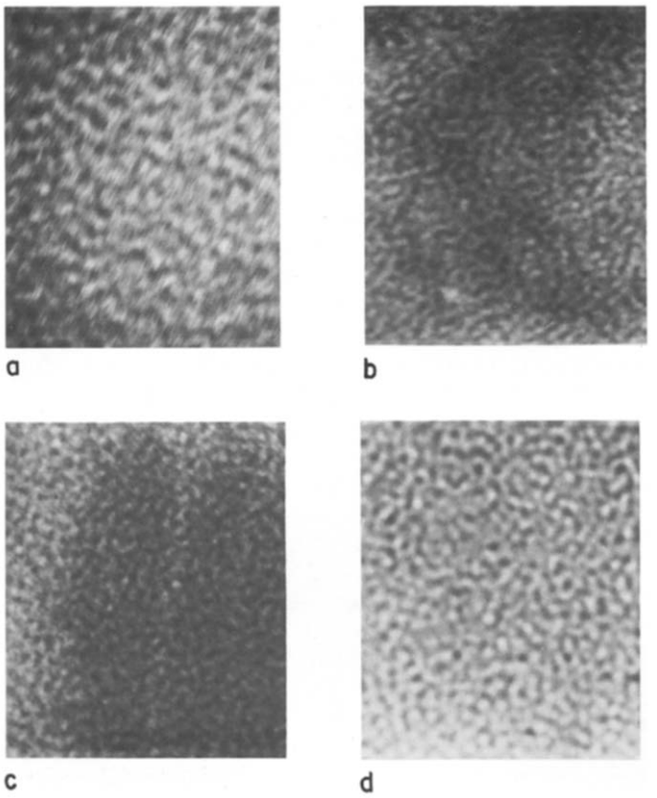

Figure 13 TEM micrographs showing the two-phase morphology in thin solution cast films for: (a) PSF4900/PSX4400 [× 300 000]; (b) PSF4900/PSX12800 [× 175 000]; (c) PSF9700/PSX12800 [× 175 000]; (d) PSF9700/PSX6700 [× 175 000]

statistically significant, fraction of relatively long blocks.

The high amplitude contrast present between the hard and soft phases also provided direct evidence by TEM of the two-phase morphology in these materials. Since the sample films were prepared by solution casting techniques, a reasonable comparison between the interdomain spacing obtained from SAXS and TEM micrographs could also be made. Such micrographs have also been obtained at this university by Patel[89] on analogous polysulphone and polysiloxane segmented copolymers. *Figure 13* shows TEM micrographs of the copolymers studied here (except in ultrathin form) and clearly provides direct visual evidence for the two-phase microstructure. A comparison of sample composition and corresponding micrographs indicates that the darker regions in the micrographs correspond to the soft siloxane phase whereas the lighter region represents the hard polysulphone phase. The images show that all samples are heterogeneous below the micron level. In general, the hard segment (PSF) regions are featureless. For PSF4900/PSX4400, *Figure 13a* shows that continuity is present for both phases, as might be expected based on composition. However, one should be cautious in postulating a specific morphology when viewing only one micrograph. Clearly, some overlap of domains probably does occur and, if so, it may provide an image of what appears as a continuous 'dark' network. When the molecular weight of the soft siloxane segments is increased in sample PSF4900/PSX12800, the interdomain spacing increases and the soft phase becomes the continuous phase (see *Figure 13b*). In *Figure 13c*, for PSF9700/PSX12800, it is found that the interdomain spacing increases even further and some continuity is present for both phases. By making several measurements of the distance between domain centres on an enlarged positive, an average interdomain spacing was calculated directly from the micrographs. The results are given in *Table 10* and show good agreement with results obtained from SAXS analysis.

Table 10 Comparison of interdomain spacing (nm) from SAXS and TEM

Sample	ID Spacing (TEM)	ID Spacing (SAXS) (Bragg)
PSF4900/PSX4400	16.0 ± 2.0	18.0
PSF4900/PSX12800	24.0 ± 2.0	21.0
PSF9700/PSX12800	36.0 ± 2.0	31.0
PSF9700/PSX6700	20.0 ± 2.0	24.0

CONCLUSIONS

Perfectly alternating segmented copolymers of polysulphone and poly(dimethylsiloxane), synthesized by solution polymerization, are transparent and show good mechanical behaviour if films are processed via solution casting. By varying the length of the segments for each phase and their relative content, it is possible to obtain a wide range of thermal and mechanical properties which are of interest as elastomers, thermoplastics and membranes. The results on the mechanical response are also influenced according to which phase is predominantly continuous.

The results from dynamic mechanical analysis confirm the two-phase nature of these copolymers. The thermomechanical spectrum showed that the nature and the extent of the rubbery plateau was affected by the choice of the segment lengths and the composition ratio.

The presence of a two-phase microstructure was also confirmed by small-angle X-ray analysis, which also allowed calculation of interdomain spacing by various techniques. As determined by Koberstein's empirical method, the values of the interfacial thickness parameter, σ, ranged from 0.8 to 1.3 nm, depending on the composition. In addition to interdomain spacing, the interfacial boundary thickness parameter and the degree of phase separation were also found to be composition dependent. The large values of interfacial thickness parameter and the level of segmental mixing obtained by SAXS analysis is somewhat surprising in view of the melt behaviour of these copolymers. However, in light of the polydispersity of the two blocks involved, the results can be explained. Finally, the results on interdomain spacing obtained from electron micrographs showed good agreement with the values obtained from SAXS.

ACKNOWLEDGEMENTS

It is a pleasure to acknowledge the financial support provided by Army Research Office through contracts ARO-DAAG29-80-K0093 and ARO-DAAG-29-84-K0091.

REFERENCES

1 Schneider, N. S., Desper, C. R., Illinger, J. L., King, A. O. and Barr, D. *J. Macromol. Sci.* (*B*) 1975, **11**, 527
2 Kimura, I., Ishihara, H. and Ono, H. *Macromolecules* 1974, **7**, 355

3 Wilkes, G. L. and Emerson, J. A. *J. Appl. Phys.* 1976, **47**, 4261
4 Koberstein, J. T. and Stein, R. S. *Polym. Sci. Eng.* 1984, **24**, 293
5 Wilkes, C. E. and Yusek, C. S. *J. Macromol. Sci. (B)* 1973, **7**, 157
6 Samuels, S. L. and Wilkes, G. L. *J. Polym. Sci., Polym. Symp.* 1973, **43**, 149
7 Ophir, Z. and Wilkes, G. L. *J. Polym. Sci., Polym. Phys. Edn* 1980, **18**, 1469
8 Paik Sung, C. S., Hu, C. B. and Wu, C. S. *Macromolecules* 1980, **13**, 111
9 Clough, S. B., Schneider, N. S. and King, A. O. *J. Macromol. Sci. (B)* 1968, **2**, 641
10 Lagasse, R. R. *J. Polym. Sci.* 1977, **21**, 2489
11 Tyagi, D., Yilgor, I., McGrath, J. E. and Wilkes, G. L. *Polymer* 1984, **25**, 1807
12 Wilkes, G. L., Bagrodia, S., Humphries, W. and Wildnauer, R. *J. Polym. Sci., Polym. Lett. Edn* 1975, **13**, 321
13 Miller, J. A., Cooper, S. L., Han, C. C. and Pruckmayr, G. *Macromolecules* 1984, **17**, 1063
14 Bates, F. S., Berney, C. V., Cohen, R. E. and Wignall, G. D. *Polymer* 1983, **25**, 519
15 Hadziioannou, G., Picot, C., Skoulios, A., Ionescu, M. L., Mathis, A., Duplessix, R., Gallot, Y. and Lingelser, J. P. *Macromolecules* 1982, **15**, 263
16 Richards, R. W. and Thompson, J. L. *Polymer* 1981, **22**, 581
17 Clough, S. B. and Schneider, N. S. *J. Macromol. Sci. (B)* 1968, **2**, 553
18 Samuels, S. L. and Wilkes, G. L. *Polymer* 1971, **9**, 761
19 Bonart, R. *J. Macromol. Sci. (B)* 1968, **2**, 115
20 Bonart, R., Morbitzer, L. and Muller, E. H. *J. Macromol. Sci. (B)* 1974, **9**, 447
21 Kimura, I., Suzuki, H., Saito, K., Watanabe, K. and Ishihara, H. *Kogyo Kagaku Zasshi* 1970, **73**, 1541
22 Assink, R. A. *J. Polym. Sci.* 1977, **15**, 59
23 Froix, M. F. and Pochan, J. M. *J. Polym. Sci.* 1976, **14**, 1047
24 Seymour, R. W. and Cooper, S. L. *Macromolecules* 1973, **6**, 48
25 Schneider, N. S. and Paik Sung, C. S. *Polym. Eng. Sci.* 1977, **17**, 73
26 MacKnight, W. J. and Yang, M. *J. Polym. Sci., Polym. Symp.* 1973, **42**, 817
27 Senich, G. A. and MacKnight, W. J. *Macromolecules* 1980, **13**, 106
28 Paik Sung, C. S., Smith, T. W. and Sung, N. H. *Macromolecules* 1980, **13**, 117
29 Estes, G. M., Seymour, R. W. and Cooper, S. L. *Macromolecules* 1971, **4**, 452
30 Lagasse, R. R. and Wischmann, K. B. *Am. Chem. Soc., Div. Org. Coat. Plast. Chem. Prepr.* 1977, **37**, 504
31 Wilkes, G. L. and Wildnauer, R. *J. Appl. Phys.* 1975, **46**, 4148
32 Hesketh, T. R., Van Bogart, J. W. C. and Cooper, S. L. *Polym. Eng. Sci.* 1980, **20**, 190
33 Miller, G. W. and Saunders, J. H. *J. Appl. Polym. Sci.* 1969, **13**, 1277
34 Koutsky, J. A., Hein, N. V. and Cooper, S. L. *J. Polym. Sci., Polym. Lett. Edn* 1970, **8**, 353
35 Wilkes, G. L., Samuels, S. L. and Crystal, R. *J. Macromol. Sci. (B)* 1974, **10**, 203
36 Chang, A. L. and Thomas, E. L. *Adv. Chem. Ser.* (Eds S. L. Cooper and G. M. Estes) 1979, **176**, 31
37 Shen, M., Mehra, U., Nieinomi, M., Koberstein, J. T. and Cooper, S. L. *J. Appl. Phys.* 1974, **45**, 4182
38 Kimura, I., Ishihara, H., Saito, K., Tamaki, K. and Ono, H. *Rep. Prog. Polym. Phys., Jpn* 1970, **13**, 209
39 Kimura, I., Ishihara, H. and Ono, H. *Macromolecules* 1971, **1**, 525
40 Fridman, I. D. and Thomas, E. L. *Polymer* 1980, **21**, 388
41 Inoue, T., Soen, T., Hashimoto, T. and Kawai, H. *Macromolecules* 1970, **3**, 87
42 Isono, Y., Tanisugi, H., Endo, K., Fujimoto, T., Hasegawa, H., Hashimoto, T. and Kawai, H. *Macromolecules* 1983, **16**, 5
43 Pedemonte, E., Turturro, A., Bianchi, U. and Devetta, P. *Polymer* 1973, **14**, 145
44 Berney, C. V., Cohen, R. E. and Bates, F. S. *Polymer* 1982, **23**, 1222
45 Hashimoto, T., Tsukahara, Y., Tachi, K. and Kawai, H. *Macromolecules* 1983, **16**, 648
46 Kato, K. *J. Polym. Sci., Polym. Lett. Edn* 1966, **4**, 35
47 Miles, M. J. and Petermann, J. *J. Macromol. Sci. (B)* 1979, **16**, 243
48 Roche, E. J. and Thomas, E. L. *Polymer* 1981, **22**, 333
49 Higgins, J. S. and Stein, R. S. *J. Appl. Crystallogr.* 1978, **11**, 346
50 Robeson, L. M., Noshay, A., Matzner, M. and Merriam, C. N. *Angew. Makromol. Chem.* 1973, **29/30**, 47
51 Hedrick, J. L., Mohanty, D. K., Johnson, B. C., Viswanathan, R. and McGrath, J. E. *Polym. Prepr.* 1983, **24**(1), 164; see also Viswanathan, R., Johnson, B. C. and McGrath, J. E. *Polymer* 1984, **25**, 1827
52 Riffle, J. S., Ph.D. Dissertation, Virginia Polytechnic Institute and State University, 1981; see also Sormani, P. M., Minton, R. J. and McGrath, J. E., in 'Ring Opening Polymerization: Kinetics, Mechanisms and Synthesis' (Ed J. E. McGrath), ACS Symposium Series No. 286, 1985, p. 147
53 Noshay, A., Matzner, M. and Merriam, C. N. *J. Polym. Sci. (A-1)* 1971, **9**, 3147
54 Noshay, A., Matzner, M. and Williams, T. C. *Ind. Eng. Chem. Prod. Res. Dev.* 1973, **12**(4), 268
55 Noshay, A., Matzner, M. and Robeson, L. M. *J. Polym. Sci., Polym. Symp. Edn* 1977, **60**, 87
56 Matzner, M., Noshay, A., Robeson, L. M., Merriam, C. N., Barclay, R. Jr and McGrath, J. E. *Appl. Polym. Symp.* 1973, **22**, 143
57 Noshay, A., Matzner, M., Barth, B. P. and Walton, R. K. *Adv. Chem. Ser.* 1976, **154**, 302
58 Wnuk, A. J., Davidson, T. F. and McGrath, J. E. *J. Appl. Polym. Sci., Appl. Polym. Symp.* 1978, **34**, 89
59 Kambour, R. P. *Polym. Prepr.* 1969, **10**, 885; see also 'Block Copolymers' (Ed. S. L. Aggarwal), Plenum Press, New York, 1970, p. 263
60 Robeson, L. M. and Faucher, J. A. *J. Polym. Sci. (B)* 1969, **7**, 35
61 Guinier, A. and Fournet, G., in 'Small Angle Scattering of X-rays', J. Wiley & Sons, London, 1955
62 Koberstein, J. T. and Stein, R. S. *J. Polym. Sci., Polym. Phys. Edn* 1983, **21**, 1439
63 Van Bogart, J. W. C., Ph.D. Thesis, University of Wisconsin, 1981 (University Microfilms 81-7545)
64 Tyagi, D., Ph.D. Dissertation, Virginia Polytechnic Institute and State University, 1985
65 Koberstein, J. T. and Stein, R. S. *J. Polym. Sci., Polym. Phys. Edn* 1983, **21**, 2181
66 Glatter, O. and Kratky, O. 'Small Angle X-ray Scattering', Academic Press, New York, 1982
67 Koberstein, J. T., Morra, B. and Stein, R. S. *J. Appl. Crystallogr.* 1980, **13**, 34
68 Helfand, E. *Acc. Chem. Res.* 1975, **8**, 295
69 Trent, J. S. *Macromolecules* 1984, **17**, 2930
70 Alexander, L. E., 'X-ray Diffraction Methods in Polymer Science', Wiley, New York, 1969
71 Handlin, D. L., Ph.D. Dissertation, University of Massachusetts, 1980
72 Odian, G., 'Principles of Polymerization', 2nd Edn, Wiley, 1981
73 Noshay, A. and McGrath, J. E., 'Block Copolymers: Overview and Critical Survey', Academic Press, New York, 1977
74 Tang, S., Meinecke, E., Riffle, J. S. and McGrath, J. E. *Rubber Chem. Technol.* 1984, **57**, 184
75 Seefried, C. G. Jr, Koleske, J. V. and Critchfield, F. E. *J. Appl. Polym. Sci.* 1975, **19**, 2493, 2503, 3185
76 Ng, H. N., Allegrezza, A. E., Seymour, R. W. and Cooper, S. L. *Polymer* 1973, **14**, 255
77 Samuels, S. L. and Wilkes, G. L. *J. Polym. Sci. (A-2)* 1973, **11**, 807
78 Huh, D. S. and Cooper, S. L. *Polym. Eng. Sci.* 1971, **11**, 369
79 Matzner, M., Noshay, A. and McGrath, J. E. *Trans. Soc. Rheol.* 1977, **21**, 273
80 Vonk, C. G. *J. Appl. Crystallogr.* 1975, **8**, 340
81 Yilgor, I., Shaaban, A. K., Steckle, W. P. Jr, Tyagi, D., Wilkes, G. L. and McGrath, J. E. *Polymer* 1984, **25**, 1800
82 Tyagi, D., Yilgor, I., McGrath, J. E. and Wilkes, G. L. *Polymer* 1984, **25**, 1807
83 Jurek, M. J. and McGrath, J. E. *Polym. Prepr.* 1985, **26**(2), 283
84 Allen, G., McAinsh, J. and Strazielle, C. *Eur. Polym. J.* 1969, **5**, 319
85 Bates, T. W., Biggins, J. and Ivin, K. J. *Makromol. Chem.* 1965, **87**, 180
86 Ivin, K. J., Ende, H. A. and Meyerhoff, G. *Polymer* 1962, **3**, 129
87 Mills, N. J. *Rheol. Acta* 1974, **13**, 185
88 Brandrup, J. and Immergut, E. H. (Eds), 'Polymer Handbook', 2nd Edn, John Wiley & Sons, New York, 1975, pp. IV–17
89 Patel, N., Masters Thesis, Virginia Polytechnic Institute and State University, 1984; Patel, N., Hedrick, J. L., Webster, D. C., Dwight, D. W. and McGrath, J. E., to be published